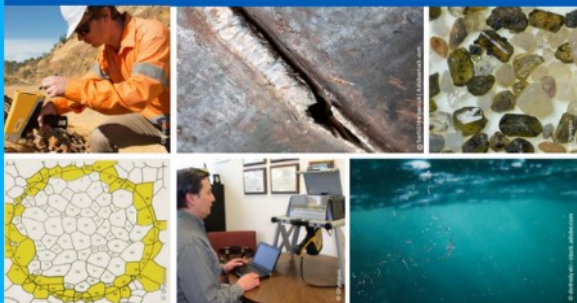




2nd Advanced Optical Metrology Compendium

Advanced Optical Metrology

Geoscience | Corrosion | Particles | Additive Manufacturing: Metallurgy, Cut Analysis & Porosity



EVIDENT
OLYMPUS

WILEY

**The latest eBook from
Advanced Optical Metrology.
Download for free.**

This compendium includes a collection of optical metrology papers, a repository of teaching materials, and instructions on how to publish scientific achievements.

With the aim of improving communication between fundamental research and industrial applications in the field of optical metrology we have collected and organized existing information and made it more accessible and useful for researchers and practitioners.

EVIDENT
OLYMPUS

WILEY

Graphene: A Reusable Substrate for Unprecedented Adsorption of Pesticides

Shihabudheen M. Maliyekkal, T. S. Sreeprasad, Deepti Krishnan, Summayya Kouser, Abhishek Kumar Mishra, Umesh V. Waghmare,* and T. Pradeep*

Unprecedented adsorption of chlorpyrifos (CP), endosulfan (ES), and malathion (ML) onto graphene oxide (GO) and reduced graphene oxide (RGO) from water is reported. The observed adsorption capacities of CP, ES, and ML are as high as ~1200, 1100, and 800 mg g⁻¹, respectively. Adsorption is found to be insensitive to pH or background ions. The adsorbent is reusable and can be applied in the field with suitable modifications. A first-principles pseudopotential-based density functional analysis of graphene–water–pesticide interactions showed that the adsorption is mediated through water, while direct interactions between graphene and the pesticides is rather weak or unlikely.

1. Introduction

Carbon and water are two vital components central to all known living systems. The adsorption capacity of several carbon forms and most importantly of activated carbon enabling affordable clean water is used extensively. The use of carbon in water purification dates back to Harappan civilization. Today, carbon has become one of the most common and

trusted means of removing contaminants like disinfection-byproduct precursors, taste and odor compounds, and synthetic organic chemicals (SOCs) such as pesticides and heavy metals from water^[1] and is the most essential component in all water purification technologies.

During the past decades, a considerable understanding of the relationship between water quality and human health has been developed. Standards of drinking water have been revised several times, and with the increased understanding of the health effects associated with several contaminants, the maximum permissible limits (MPL) of contaminants are likely to reach molecular limits in due course.^[2] Among the 92 regulated contaminant species as per the environmental protection agency (EPA) guidelines, pesticides are of major concern due to their indiscriminate use and widespread presence in drinking water. The toxicity and health hazards posed by pesticides, even at very low concentrations, have become large concerns for both developing and developed countries.^[3,4] World health organization (WHO) drinking water standards prescribe an MPL for a single pesticide as 0.1 µg L⁻¹. It is in this context that new adsorbents and new chemistry have to be developed to control these species. As a result of this tireless search for new technology to enable the efficient separation of pesticides from water, many new materials with interesting properties have been developed. We have reported the use of noble metal nanoparticles for the degradation of pesticides in water at ultra low concentrations^[5] and introduced this technology in the market.^[2]

Dr. S. M. Maliyekkal, Dr. T. S. Sreeprasad,
D. Krishnan, Prof. T. Pradeep
DST Unit on Nanoscience
Department of Chemistry
Indian Institute of Technology Madras
Chennai - 600 036, India
Fax: 91-44-2257-0545/0509
E-mail: pradeep@iitm.ac.in

Dr. S. M. Maliyekkal
School of Mechanical and Building Sciences
VIT University
Chennai Campus, Chennai-600 127, India
S. Kouser, Dr. A. K. Mishra, Prof. U. V. Waghmare
Theoretical Sciences Unit
Jawaharlal Nehru Centre for Advanced Scientific Research (JNCASR)
Jakkur, Bangalore 560 064, India
E-mail: waghmare@jncasr.ac.in



DOI: 10.1002/sml.201201125

Carbon nanotubes (CNTs) are another category of materials investigated recently for pesticide uptake.^[6–8] Studies demonstrated that CNTs are promising candidates for the adsorption of a few SOC from water and the adsorption capacities are dependent on various factors including the specific surface area and pore volume of the CNTs, the density of oxygen-containing functionalities on CNTs, and the chemical nature of the pollutant. However, CNTs are reported to be cytotoxic,^[9,10] which may limit their utility in drinking water purification.

Since the discovery of graphene—a single atomic layer of carbon—in 2004,^[11] it has attracted overwhelming attention due to its unique chemical and physical properties and low production cost compared to other graphitic forms.^[12–14] As of now, graphene and graphene-based materials have been proposed for many applications. This includes drug delivery,^[15] solid-state gas sensors,^[16] electrochemical sensors,^[17,18] Raman scattering-based molecular sensors,^[19] hydrogen storage,^[20,21] energy storage devices,^[22] and catalysis.^[23] Recent studies show that graphene-based materials have good potential in environmental cleanup as well. Large surface area,^[24] reduced cytotoxicity,^[25] the large delocalized π electrons^[26] and tunable chemical properties^[27] make these materials perfect candidates for the adsorption of chemicals and thus the cleanup of water. The utility of graphene-based materials for arsenic removal has been proved very recently.^[28] The antibacterial properties of graphene oxide (GO) and reduced graphene oxide (RGO) have also been studied and it has been found that both are antibacterial.^[25] Sreeprasad et al. have reported a new methodology to make a series of RGO–metal and –metal oxide composites and studied their application for Hg(II) removal from water.^[29] The study also showed a simple method to immobilize GO/RGO on sand particles and demonstrated the utility of this material in heavy metal removal. Gao and co-workers also demonstrated that GO-coated sand could be used as a low-cost water purification material for developing economies.^[30] A recent investigation shows that sulfonated graphene is a good medium for the separation of naphthalene and 1-naphthol from water and the adsorption capacities were estimated to be ~ 2.3 – 2.4 mmol g^{−1}.^[31] However, no systematic effort has been done to use RGO and GO to remove complex molecules such as pesticides from water. Considering the diverse nature of pollutants in water, we believe that continuous and systematic efforts are needed to bring advanced materials like graphene for down-to-earth applications like water purification. To the best of our knowledge, no theoretical investigation is available in the literature to explain the phenomenon of organics–water–graphene interactions. Such studies may help to understand the system better and thus allow fine tuning for improved performance.

In this paper, we explore the use of RGO and GO for the removal of pesticides like endosulfan (ES), chlorpyrifos (ES), and malathion (ML) from water under different conditions. In order to delineate the removal mechanism and to comprehend the observed uptake capacity, an analysis using first-principles pseudopotential-based density functional theory (DFT) was carried out. The pesticides used in this study are widely detected in the surface and groundwaters

of many countries.^[32] While ES belongs to the organochlorine (OC) group, CP and ML belong to the organophosphate group, which are second generation pesticides developed as substitutes to OC pesticides. Although many OC pesticides are prohibited, ES is still used extensively as an insecticide in countries such as India, Pakistan, and Bangladesh under different trade names like Thiodan, Thionex, and Endosan.^[33a] Endosulfan is one of the most commonly detected pesticides in surface waters of the US (38 states).^[33b] CP (trade names: dursban, lorsban, agromil, dhanwan, dorson, dhanwan, omexan, etc.) and ML are reported to be used both for agricultural and landscape pest control and their presence in water is widely reported.^[32a,32c] The toxic effects of these pesticides are well documented.^[34]

2. Results and Discussion

2.1. Characterization of GO and RGO

The UV–vis spectral features of GO and RGO are shown in **Figure 1A**. The absorption peak at 232 nm showed the typical characteristic of GO and red shift in the peak (at 268 nm) after reduction confirmed the transformation of GO to RGO. The attenuated total reflectance infrared spectroscopy (ATR-IR) spectra of GO and RGO are shown in the inset of **Figure 1A**. GO showed characteristic peaks at 1217 (epoxy C–O), 1415 (carboxy C–O), 1614 (aromatic C=C), and 1720 (C=O in carboxylic acid), and 1035 cm^{−1} (epoxy or alkoxy C–O). The broad band between 3200–3400 cm^{−1} can be attributed to O–H stretching vibrations. In the case of RGO, most of the peaks due to oxygen functionalities disappeared. The peak at 1415 cm^{−1} almost vanished after reduction. The peaks at 1575 and 1100 cm^{−1} are due to the aromatic C=C and C–O stretching vibrations, respectively.^[35] Raman spectra of GO and RGO were also collected. As shown in **Figure 1B**, the Raman spectrum of GO showed the D-band at 1345 cm^{−1} and G-band at 1609 cm^{−1}. After reduction, the D-band position remained the same but G-band shifted to a lower frequency region (1590 cm^{−1}), confirming the reduction of GO to RGO.^[36]

GO and RGO were characterized by X-ray photoelectron spectroscopy (XPS) as well. **Figure 1C** shows the XPS spectra of GO and RGO. GO showed four components in the C 1s spectrum. The prominent peak centered on 284.5 eV is attributed to nonoxygenated ring C 1s. Other three peaks centered around 288.8, 287.6, and 286.3 eV are ascribed to C(O)O, C=O and C–O, respectively.^[36] After the reduction of GO, the C 1s spectrum showed a major peak centered around 284.6 eV, corresponding to a non-oxygenated ring carbon. The peak centered at 288.9 eV is assigned to C(O)O. Evidently, the oxygenated peak at 286.3 eV due to C–O disappeared completely. High-resolution transmission electron microscopy (HRTEM) image of RGO sheets is shown in **Figure 1D**. An enlarged portion showing the thin folding is given in the inset. The graphenic nature of the materials can be seen from the characteristic ripples present on the sheets of GO and RGO. The edges and wrinkles were measured to

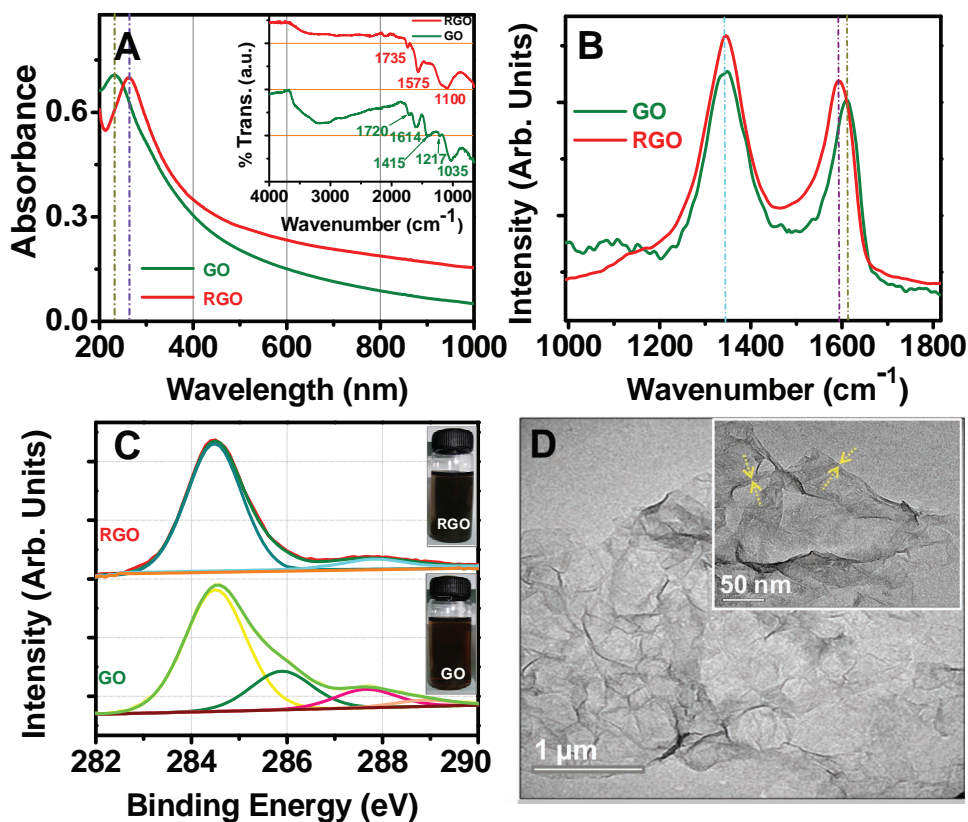


Figure 1. (A) UV-vis, (B) Raman, and (C) XPS spectra of GO and RGO. (D) HRTEM image of RGO. Inset of A shows ATR-IR of GO and RGO. Traces are shifted vertically for clarity. The shift in G-band is shown with vertical lines. Inset of (C) shows the photographs of RGO and GO dispersed in DW. Inset of (D) shows a magnified HRTEM image of RGO. The characteristic wrinkles of RGO are marked on the figure.

be around $\sim 1\text{--}1.5$ nm thick, which is close to a bilayer thickness (inset Figure 1D).^[37] RGO samples were analyzed by scanning electron microscopy and energy dispersive microscopy (SEM-EDAX) as well. A representative EDAX spectrum and elemental maps obtained are shown in Figure S3 of the Supporting Information. An SEM image of RGO from which the EDAX spectrum and maps for certain elements of relevance to pesticides were taken is also given in Figure S3. The data reveal that the sample is devoid of impurities.

2.2. Adsorption Studies

2.2.1. Comparison of GO and RGO for the Removal of Pesticides

Both GO and RGO were tested for the removal of pesticides at room temperature and neutral pH and the data for CP is shown in Figure 2. Unit uptake capacities of CP increased with decreasing RGO or GO dose. This might be due to increased mass transfer at higher adsorbate to adsorbent ratio. Better separation of RGO or GO sheets at higher dilution and thereby increased available surface area could be another reason for the significant increase in uptake capacity at lower doses. The data also revealed that RGO is a better candidate compared to GO in adsorbing CP from water. The CP uptake capacity of RGO was found to be as high as ~ 1200 mg g⁻¹, approximately 10–20% higher than that of GO. To

the best of our knowledge, no adsorbents used for the purpose are reported to have adsorption capacities of more than the weight of the adsorbate, and therefore this observation is unprecedented. Similar adsorption trends were observed for the other pesticides as well, i.e., ES and ML (Supporting Information, Figure S4). The observed capacities are several times higher than the adsorption capacities of various adsorbents investigated for the purpose.^[38–40]

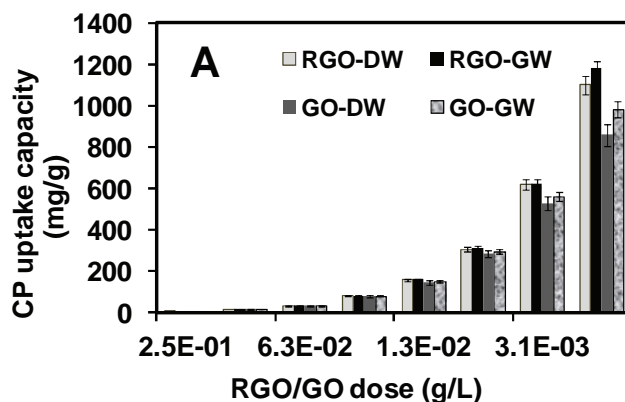


Figure 2. Adsorption of CP as a function of RGO and GO dose. Initial concentration of CP ≈ 2 mg L⁻¹, pH = 7 ± 0.2 , and temperature = 30 ± 2 °C.

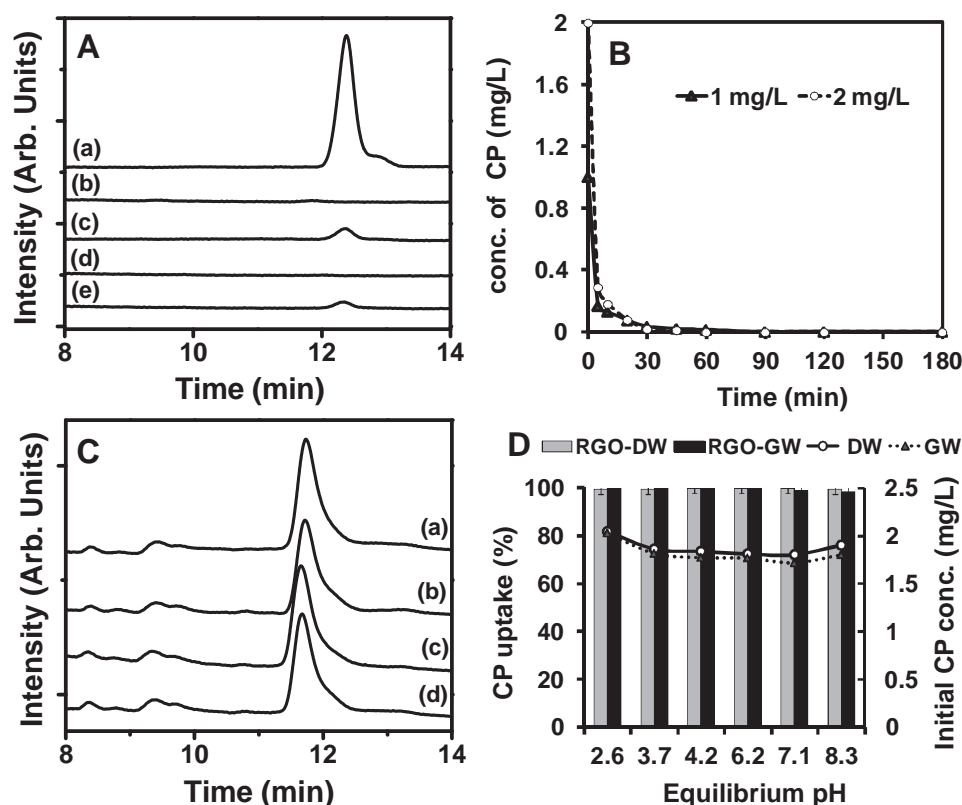


Figure 3. A) HPLC traces of (a) initial 2 mg L^{-1} of CP; (b) residual CP after contact with RGO dispersed in DW, and; (c) GO dispersed in DW; (d) residual CP after contact with RGO dispersed in GW, and (e) GO dispersed in GW. B) Time-dependent removal of CP by RGO at two different initial concentrations of CP. C) HPLC traces of initial and desorbed CP; a, b, c, and d show initial CP and CP desorbed in three consecutive desorption cycles, respectively. D) Effect of pH on the adsorption of CP by RGO. Line diagrams (axis on the right) show the measured initial concentrations of CP at various pHs. RGO–DW indicates RGO dispersed in deionized water spiked with pesticide; RGO–GW indicates RGO dispersed in groundwater spiked with pesticide.

In order to study the interference of other ions on pesticide removal, adsorption studies were also done in groundwater spiked with pesticides. **Figure 3A** shows the High performance liquid chromatography (HPLC) trace of CP before and after contact with 0.0125 g L^{-1} of RGO. The corresponding HPLC spectra of ES and ML are given in Figure S5 of the Supporting Information. The data showed no interference, irrespective of the pesticides studied, and thus proved the possible utility of RGO and GO in purification of real waters.

2.2.2 Adsorption Kinetics

The rate of adsorption is an important factor in any adsorption process. It varies with the physical and chemical properties of the adsorbent. Here, the time dependent adsorption of CP, ES, and ML onto RGO was tested and the data for CP are given in Figure 3B. The data for ES and ML are given in Supporting Information, Figure S6. The kinetic data exhibited rapid removal of pesticides. More than 90% of the pesticide removal happened in <10 min contact time, and no traces of pesticide were detected after 30 min of contact with RGO. Control samples were also run to account for any possible volatilization and hydrolysis and they showed an insignificant effect. Concentration variation in the control was estimated to be less than 5%.

2.2.3. Regeneration and Reuse

For checking the reuse potential of RGO, successive adsorption–desorption cycles were conducted. The reuse capacity was studied for three consecutive cycles of adsorption–desorption. The HPLC spectra obtained during three desorption cycles are shown in Figure 3C. The percentage removal of CP for the corresponding adsorption cycle is shown in Figure S7 of Supporting Information. More than 90% desorption and insignificant reduction in CP uptake capacity was seen with repeated use. In the course of the study, we also observed that a good portion of RGO, which is initially dispersed in water, came to the water–hexane interface, indicating the nonpolar nature of the RGO. However, we could re-disperse the RGO effectively by ultrasonication. The UV features of the cycled RGO were also collected (Figure S7). No significant change in spectral features was seen, indicating that RGO is intact even after repeated use.

2.2.4. Effect of pH on Adsorption

The pH of the solution plays an important role in the adsorption process since it can alter the solute species as well as the surface properties of the adsorbent. At a given pH, the adsorbate and adsorbent may co-exist such that the same

or opposite charges may be present. The pesticides are susceptible to hydrolysis in aqueous media and can result in some new species, different from the parent compound. It is reported that pesticides like CP, ES, and ML hydrolyze at a faster rate in alkaline pH, whereas no effect on hydrolysis was reported at acidic pH.^[41,42] Here, RGO was tested for the pesticide uptake from water, both DW and GW, as a function of pH under batch equilibrium conditions. Figure 3D shows insignificant variation in CP uptake capacity over the pH range studied (pH \approx 3–9). Similar behavior was observed with ML and ES as well (data not shown). None of the pesticides studied are ionizable, indicating that the pesticides behave as electroneutral species. Hence, the interaction between the adsorbate and adsorbent is not expected to change with pH.^[43,44] Therefore, the interaction of a neutral molecule with a relatively electroneutral surface of RGO should show a pH-independent adsorption pattern. Analysis of the initial pesticide samples also show no evidence of the formation of hydrolysis products over the experimental time span. A study on the adsorption of diuron, a non-polar pesticide, by carbon, shows a pH-independent adsorption.^[44] The same group also reported that pesticide adsorption varies with the surface functionality of the adsorbent as well as the ionic nature of the pesticide.

The pH-independent adsorption behavior of RGO indicates that the surface functional group ($-\text{COO}^-$) present on the RGO surface is not involved in the adsorption of pesticides. This may suggest the absence of direct interactions of the pesticide with RGO in the adsorption process.^[45]

2.3. Characterization of RGO After Contact With the Pesticide Samples

The adsorption of pesticides onto RGO was also illustrated using desorption electrospray ionization (DESI) mass spectrometry measurements. CP on glass plate showed its characteristic molecular ion at m/z 352 (Supporting Information, Figure S8A). Collision-induced dissociation of this ion (in mass spectrometry/mass spectrometry (MS/MS)) confirmed the identity of the species (inset of Supporting Information, Figure S8B). RGO loaded with CP showed the characteristic molecular ion peak at m/z 352 (Figure 4A). The isotope pattern exhibited by this peak is similar to the theoretically predicted pattern, confirming the presence of CP on RGO. The MS/MS measurement further confirmed the identity of the species (Figure 4B). The fragmented ion at m/z 324 is due to the loss of C_2H_4 from the molecular ion at m/z 352. The subsequent loss of C_2H_4 from m/z 324 resulted in the ion

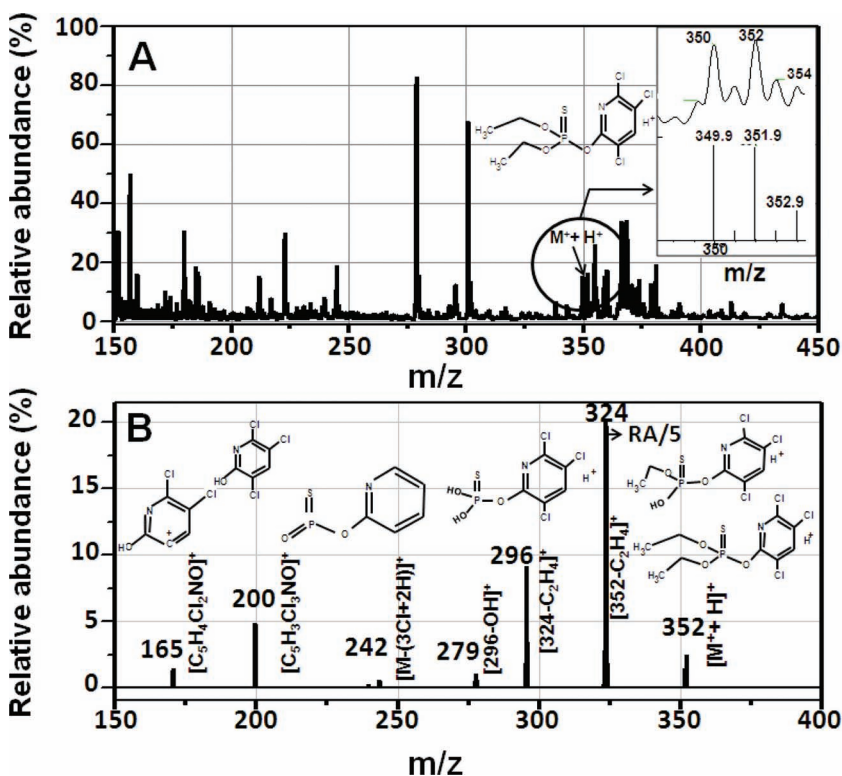


Figure 4. (A) Positive ion DESI mass spectrum of CP on RGO surface. (B) MS/MS analysis of m/z 352. Inset of A shows an expanded view of the molecular ion peak and a comparison with the theoretical isotope pattern. The m/z 324 peak intensity (RA) in B is multiplied by 1/5 to show all the ions clearly.

at m/z 296. The fragmented ion at m/z 200 was assigned to $[\text{C}_5\text{H}_3\text{Cl}_3\text{NO}]^+$.

The mass spectra of ML were also recorded and the data showed the molecular ion peak at m/z 331 (Supporting Information, Figure S9A). The theoretical and experimental isotope pattern exhibited by the molecular ion peak showed 1:1 correspondence, confirming the presence of ML on RGO (inset of Figure S9A). The MS/MS spectrum of the molecular ion is shown in Supporting Information, Figure S9B. The fragment ion masses and their molecular formulae are marked in the figure. The data established the presence of adsorbed ML on RGO.

Figures 5A and B show the TEM and SEM images, respectively, of RGO after adsorption of CP. We can see that the thickness of the sheet increased after pesticide adsorption. Similar observations were seen in the case of other pesticides as well (Supporting Information, Figure S10). However, the shape of the sheet was preserved and RGO remained in suspension without any visible aggregation. This may be explained as follows: It is known that GO prepared through reduction route can form well-dispersed aqueous colloids. The stability is attributed to electrostatic repulsion due to high surface negative charge generated as a result of ionization of the $-\text{COOH}$ and $-\text{OH}$ groups on the GO sheets.^[36] It is also known that $-\text{COOH}$ groups are unlikely to be reduced under these experimental conditions, indicating that the surface of RGO is still negatively charged. Adsorption of non-ionic species like CP, ES, and ML is unlikely to change

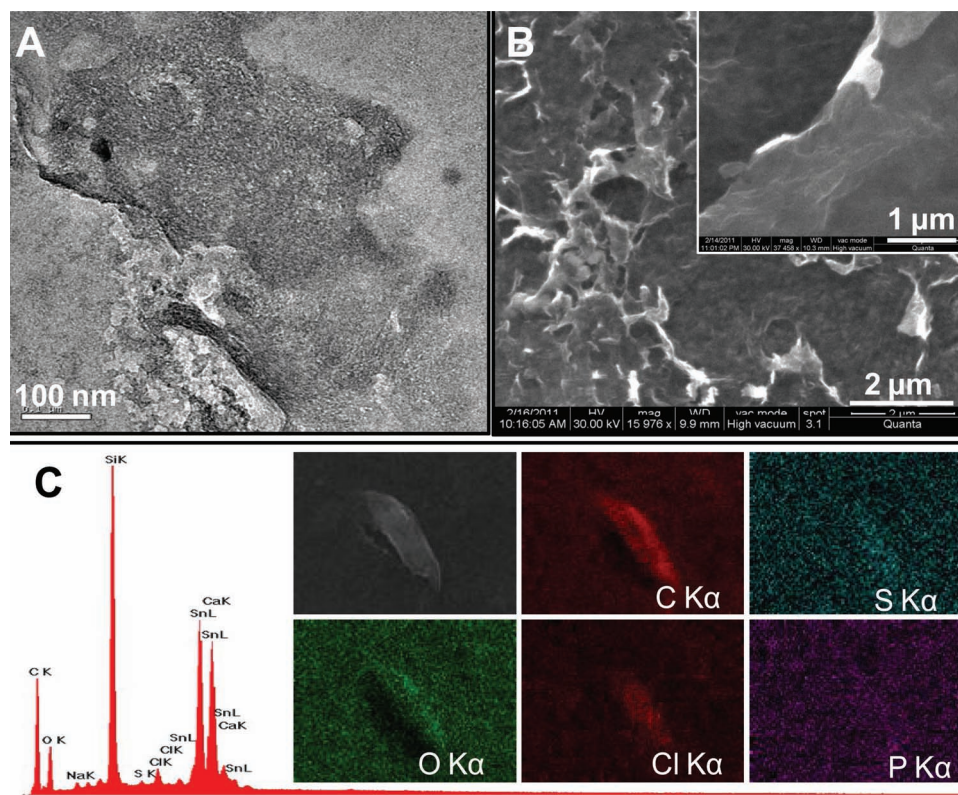


Figure 5. (A) TEM image of RGO after adsorption of CP. (B) SEM image of RGO after adsorption of CP. Inset of (B) shows a magnified SEM image. (C) EDAX spectrum of RGO loaded with CP. Inset of (C) shows the X-ray images of various elements present in RGO along with a SEM image.

the surface charge and hence the stability. On the contrary, aggregation of RGO was observed in groundwater spiked with pesticides. This may be due to the interaction of cations present in groundwater with negative functional groups on RGO, i.e., COO^- , and thereby charge neutralization and coagulation. The flocs once formed can be redispersed temporarily by ultrasonication.

2.4. First-Principles Analysis of the Graphene, Pesticide and Water Interactions

We now present results to address the following issues in the observed capacity of graphene to adsorb these pesticides at unprecedented levels: 1) Is adsorption feasible and how is it influenced by water? 2) Is such a large capacity of adsorption possible, and what may the upper limit be? 3) What are the atomistic mechanisms responsible?

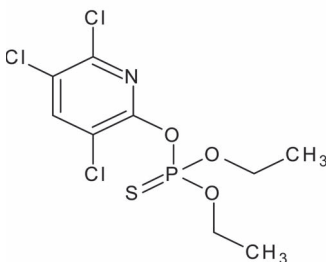
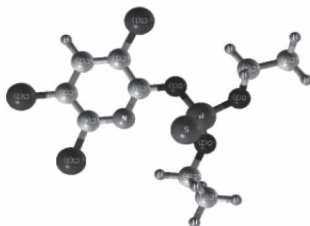
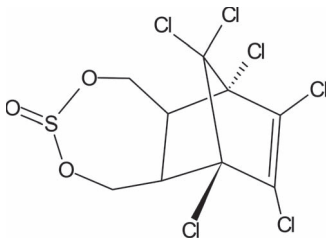
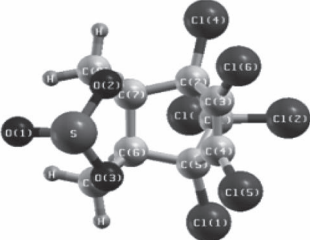
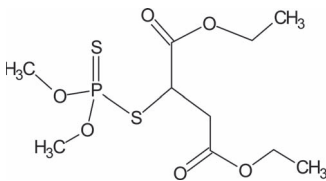
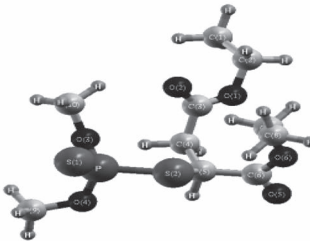
While all experiments were carried out at room temperature, the first-principles calculations provided energies at 0 K, and we used them to develop a qualitative understanding of our experiments. Although such calculations can be employed in molecular dynamics to simulate behavior at finite temperature, this approach is quite expensive and unrealistic, particularly to access the time-scales relevant to the separation of pesticides from water. However, to have some idea about entropic effects, we have considered various (8 to 10) configurations for different aggregates or complexes of

water, graphene, and each of the three pesticide molecules. To facilitate a comparative analysis of the energetics that involve different species of atoms, we first considered the following systems: a free water molecule (W), pristine graphene (G), a free pesticide molecule ($P = \text{ES}, \text{CP}, \text{or ML}$), and an aggregate of n water molecules (nW). The energy of each of these was determined through structural relaxation in a large supercell. Our optimized structure of graphene has a lattice constant of 2.45 Å, in good agreement with the experimental value of 2.46 Å.^[46] Using an experimental^[47] hexagonal crystal structure of β -ES for the initial guess in our structural optimization, we found that bond-lengths of ES change by only a couple of percent during relaxation, within the typical errors of DFT calculations. Similarly, we used a monoclinic crystal structure of CP generated experimentally^[48] and found that our calculated structure is in reasonable agreement with experiment. A detailed structure of ML is not available experimentally, so we determined it from our calculations. Since our pseudopotentials and other calculational parameters accurately described the structures of ES and CP, we expect a similar level of accuracy in the structure of ML (see theoretical structures of pesticides in **Table 1**).

2.5. Adsorption of Pesticide on Graphene

Among the binary complexes, we first considered different (3–4) configurations of pesticide–graphene (P–G) complexes

Table 1. Selected properties of the pesticides used in the study.

Pesticide	Molecular Formula	Chemical Structure	Theoretical Structure (From DFT Calculations)	Mol. Wt. [g mol ⁻¹]	Water solubility [mg L ⁻¹]
Chlorpyrifos (C ₉ H ₁₁ Cl ₃ NO ₃ PS)					
Chlorpyrifos [O,O-diethyl-O-(3,5,6-trichloro-2-pyridyl)phosphorothioate]	C ₉ H ₁₁ Cl ₃ NO ₃ PS			350.59	2 (25 °C)
Endosulfan [6,7,8,9,10,10-Hexachloro-1,5,5a,6,9,9a-hexahydro-6,9-methano-2,4,3-benzodioxathiepin-3-oxide]	C ₉ H ₆ Cl ₆ O ₃ S			406.93	α-ES- 0.32 β-ES- 0.33 (22 °C)
Malathion [diethyl 2-[(dimethoxyphosphorothioyl)sulfonyl]butanedioate]	C ₁₀ H ₁₉ O ₆ PS ₂			330.36	130 (25 °C)

with different orientations of each pesticide with respect to the graphene sheet (see their relaxed structures in **Figure 6A** and Figure S11A of Supporting Information). To quantify the strength of the interactions between P and G, we obtained an adsorption energy, E_A defined as defined in equation 1.

$$E_A = E_{P-G} - (E_P + E_G) \quad (1)$$

where, E_{P-G} , E_P , E_G are the energies of the optimized structures of pesticide-graphene complex, isolated free pesticide molecule, and graphene supercell, respectively. Similarly, we quantify the energy of dissolution as defined in equation 2.

$$E_D = E_{W-G/P} - (E_W + E_{G/P}) \quad (2)$$

where $E_{W-G/P}$ is the energy of the water and graphene or water and pesticide complex. Our results clearly reveal that $E_A > 0$ with magnitudes from 30 to 50 kJ mol⁻¹ for ES and CP, while there is weak binding (−2 to −3 kJ mol⁻¹) for ML, and thus adsorption of these pesticides on dry graphene is unlikely or at the best very weak (Supporting Information, Table S12), and that $E_D < 0$ meaning both graphene and pesticide have an attractive interaction with water molecules (relative to free water molecules). However, we also found

that $E(nW) - nE(W) < 0$, with a magnitude comparable and even greater than that of E_D in the case of ML and CP. Thus, the adsorption of pesticides or graphene in water is limited. Experimental samples of graphene here, though, are partially functionalized which can alter the adsorption of graphene.

Finally, we turn to our results on ternary G–W–P complexes (Supporting Information, Table S13). To evaluate energetic stability, we examine the adsorption energy of the G–W–P complex (see their structural configurations in Supporting Information, Figures S11B and S14) as defined in equation 3.

$$E_{G-W-P} = E_{complex} - (E_G + E_P + nE_W) \quad (3)$$

for $n = 6$, and compare with E_A and E_D defined earlier. First of all, we find that there is an energy gain associated with binding between graphene, pesticide, and water molecules relative to any of the pair complexes: $E_{G-W-P} < E_A$ and $E_{G-W-P} < E_D$, when we consider the lowest energy configuration for each. For each pesticide, the energy of the G–W–P complex is lower by 20–40 kJ mol⁻¹ than the energy of a pair complex such as W–P or W–G or nW ($n = 6$). Thus, with respect to free graphene or free pesticide in water, it is energetically preferable for a G–W–P complex to exist. Secondly,

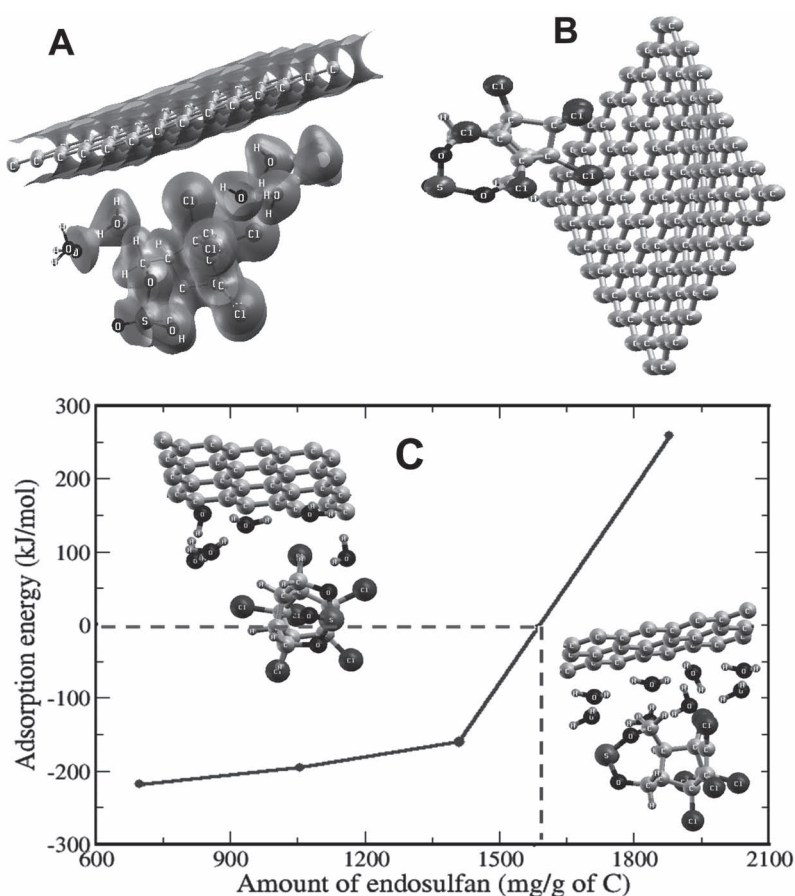


Figure 6. Relaxed structure of (A) G-W-ES complex and (B) ES-G complex. (C) Energy of adsorption of endosulfan on graphene in the presence of water molecules as a function of coverage (expressed in amount of ES per gram of graphene). The structure on the left corresponds to a 4×4 supercell and good binding in the complex, while the one on the right is for a 3×3 supercell of graphene with no binding.

the energy gain associated with the formation of a graphene–pesticide–water complex increases with n (Supporting Information, Table S15), up to a value that gives a reasonable packing of water molecules in the space available (about $n = 50$, depending on the pesticide) in the 5×5 supercell. We find that only a few bonds, particularly the polar ones, in a pesticide molecule, which are close to water molecules and graphene, change noticeably when it enters into an interaction with graphene and water. For example, while one of the P–S bonds in ML elongates and the other shortens by 1%, both P–O bonds contract by less than a percent. While a P–S bond in CP elongates by a percent, its P–O bonds are shortened by less than a percent. In ES, one of the S–O bonds becomes longer by a percent and the other contracts by half a percent. As the distance between any of the molecules and graphene is always greater than a typical bonding distance, we conclude that the origin of these structural changes and associated energetics is mainly electrostatic in nature. Visualization of the structure and charge density (Figure 6A) reveal polarity and suggest an electrostatic interaction. Naturally, water, with its polar structure, plays an important role in mediating effective interactions between graphene and a pesticide. The nature of interaction between dry graphene

and ES is slightly different, and involves some bending (by 3.2°) of graphene sheet (Figure 6B) and costs energy of the order $30\text{--}50\text{ kJ mol}^{-1}$. In this case, the S=O (double bond) bonds elongate by 1.7% and both single S–O bonds elongate by 3.5% relative to the relaxed ES molecule. On the other hand, one of the C–Cl bonds closer to the graphene sheet shortens by 1%, and the other elongates by 3.5%.

Our calculations with $n \times n$ supercell of graphene correspond to pesticide adsorption capacities ranging from 600 to 2000 mg g^{-1} (Supporting Information, Table S16). Our results for G-W-ES (Figure 6C) clearly show that there is an overall binding between ES, graphene, and water molecules for coverages lower than 1600 mg g^{-1} . Indeed, this confirms the experimental observation that a pesticide can precipitate along with graphene and water at these high coverages/capacities. Our theoretical estimate of the upper limit on pesticide adsorption capacity is slightly higher than the experimental value because it corresponds to the most stable configuration ($T = 0\text{ K}$) among the ones considered here, and DFT calculations are known to typically overestimate the binding energies.

3. Conclusion

Unprecedented water-assisted adsorption of common pesticides on graphene is demonstrated here with a combination of theory and experiment. Our work establishes that the new class of 2D carbon nanomaterials has enormous potential in water purification, in creating cheap, easily manufacturable substrates. The adsorption capacity of graphene observed to be as large as 1200 mg g^{-1} is higher than any materials investigated for the purpose. The material is also attractive due to its high specificity to the pesticides, insensitivity to changes in pH, less toxicity compared to other carbon-based nanomaterials like CNTs, and antibacterial properties (consequently unlikely accumulation of bacteria on the filter media). Besides the said merits, RGO can be easily immobilized on cheap substrates like sand and used as a filter that reduces many engineering limitations of the said material in applications like water purification. Using first-principles DFT-based analysis, we have determined the energies of adsorptive interactions between graphene and a pesticide (binary complex) as well as graphene, pesticide, and water complexes, revealing that the pesticide adsorption on graphene is thermodynamically feasible only in the presence of water molecules, and the adsorption of any of the three pesticides on dry graphene is expected to be rather weak or unlikely. Hence, the observed removal of pesticides from water by graphene is proposed to be due to the formation

and precipitation of G–W–P complexes through electrostatic interactions. The present study reveals the richness in interactions of graphene with molecular systems and opens a way for further research in this important field of environment friendly applications of graphene.

4. Experimental and Computational Details

Materials: Natural graphite was purchased from Active Carbon India Pvt. Ltd., India. Hydrochloric acid (HCl, 36%), ammonia (NH₃, 30%) and sulfuric acid (H₂SO₄, 95–98%) were procured from Rankem Chemicals, India. CP (HPLC assay 99.9%), ES (HPLC assay 99.9%, $\alpha:\beta = 1:2$), and ML (HPLC assay 96.1%) were purchased from Sigma Aldrich. Stock solutions of the pesticides were prepared in high pure ethanol (99.9%) and maintained under refrigeration until needed for testing. Phosphorus pentoxide (P₂O₅), hydrazine monohydrate (N₂H₄·H₂O, 99–100%) and hydrogen peroxide (H₂O₂), were purchased from SD Fine Chemicals, India. Potassium peroxydisulfate (K₂S₂O₈) was purchased from Sisco Research Laboratories Pvt. Ltd., India. Potassium permanganate (KMnO₄) was purchased from Merck. All chemicals were used as received without any additional purification. All solutions and suspensions were prepared using deionized water (DW).

GO and RGO Synthesis: GO synthesis from graphite powder was carried out based on the modified Hummers method.^[49] RGO synthesis was done by chemical reduction of GO as reported by Li et al.^[50] as well as through hydrothermal reduction method reported by Zhou and co-workers.^[51] The detailed procedure is given in Supporting Information S1. Various concentrations of RGO and GO were prepared by appropriate dilution using DW. The samples were dialyzed against DW to get rid of ionic impurities. After dialysis, the samples were stored in glass bottles for further use.

RGO prepared through two different reduction routes were tested for their adsorption capacity. This was done to study the influence of reduction processes on adsorption. Chemical reduction can leave reductants with graphene and its influence on adsorption was an important aspect of the investigation. The results revealed that the reduction methodologies have an insignificant effect on the adsorption process. All the experiments reported in the paper were carried out using hydrothermally synthesized RGO.

Adsorption Experiments: The pesticide uptake capacities of GO and RGO dispersions were investigated in a batch reactor (20 mL). The working volume was maintained at 10 mL. Homogeneous dispersions of GO and RGO were taken in the reactor separately and the target pesticide was added into the dispersion to get the required concentration of the contaminant. All the adsorption experiments were conducted at room temperature (30 ± 2 °C). Selected properties of the pesticides used in this are given in Table 1.

The solutions contained a small amount of ethanol (<0.5% by volume), which was added with the pesticide stock solution. The solutions were kept for stirring at ambient conditions. The solid–liquid separation was done by membrane filtration. The filtrate was analyzed to quantify the target pesticide in the aqueous phase by high pressure liquid chromatography (HPLC) (Dionex, UltiMate 3000) equipped with an UltiMate 3000 variable wave length detector and a packed column of Agilent C18, 100A. CP analysis

was carried out at a wavelength of 267 nm. An acetonitrile:water (80:20) mixture was used as the mobile phase and a total flow rate of 1 mL min^{−1} was maintained. ES and ML were analysed at similar settings but at a wavelength of 214 nm. The effects of pH, contact time, adsorbent dose, and co-existing ions were evaluated by varying the parameters in the appropriate window. Except kinetics, all other studies were conducted by a batch equilibration method. For conducting adsorption experiments in real water, the water was simulated by spiking the required concentration of target pesticide into groundwater (GW). The water quality characteristics of the groundwater are given in Supporting Information (Table S2 of Supporting Information). Control samples were kept in all the cases to assess the removal of the pesticides by methods other than adsorption by RGO/GO. All the experiments were conducted in duplicate with proper control and the samples were analyzed immediately.

Regeneration Studies: Once used RGO was regenerated using n-hexane as the eluent. The test was restricted to CP@RGO alone (@ implies CP adsorption on RGO), since all the three pesticides studied showed similar behaviour. To begin with, CP (2 mg L^{−1}) was initially equilibrated with a dispersion of RGO (10 mL) at neutral pH and at room temperature (30 ± 2 °C). After achieving equilibrium, n-hexane (5 mL) was added to the reactor and stirred for 30 min. After 30 min, n-hexane (4 mL) was separated from the reactor carefully and the solvent was evaporated by means of rotary vaporisation. The pesticide residue was re-dissolved in equal volume of ethanol (4 mL) and analyzed using HPLC as described above. After the first cycle, the RGO was separated from the solvent and reused for the subsequent adsorption and desorption cycles.

Instrumentation: UV–vis spectra of GO and RGO were measured using a Perkin-Elmer Lambda 25 UV/Vis spectrophotometer. Attenuated total reflectance-infrared (ATR-IR) measurements were done using a PerkinElmer, Spectrum 100 spectrometer. Raman spectra of GO and RGO were collected using a confocal Raman spectroscopy (WiTec GmbH CRM 200). X-ray photoelectron spectroscopic (XPS) measurements were done with an Omicron ESCA Probe spectrometer with unmonochromatized Mg K_α X-rays (hν = 1253.6 eV). The energy resolution of the spectrometer was set at 0.1 eV at a pass energy of 20 eV. Binding energy was corrected with respect to C 1s at 284.5 eV. A high-resolution transmission electron microscope (HRTEM) with an ultra-high resolution (UHR) polepiece was used to image the samples (JEOL 3011, 300 kV). Surface morphology, elemental analysis and elemental mapping studies were carried out using scanning electron microscopy (SEM) equipped with energy dispersive analysis of X-rays (EDAX) (FEI Quanta 200, Czechoslovakia). The samples were analyzed using an electrospray ionization mass spectrometer (LTQ XL, Thermo Scientific, San Jose, CA) equipped with a 2D moving stage (Prosolia, Indianapolis, IN) desorption electrospray-mass spectrometry (DESI-MS) imaging. All the mass spectra were acquired under identical conditions of 2 mL min^{−1} solvent flow rate, 110 psi nebulizer gas (N₂) pressure, and 5 kV spray voltage.

First-Principles DFT Analysis of Graphene, Pesticide and Water Interactions: We used Plane-Wave Self-Consistent Field (PWSCF)^[52] implementation of DFT, which is based on ultra-soft pseudopotentials^[53,54] to represent interactions between ionic cores and valence electrons and a plane-wave basis. As the densities in molecular systems change rapidly in space, we used a generalized gradient approximation (GGA) with Perdew–Burke–Ernzerhof

(PBE)^[54] form of the exchange correlation energy functional. Kohn–Sham wave functions were represented with a plane wave basis with an energy cutoff of 30 Ry and charge density with a cutoff of 180 Ry. We used periodic boundary conditions with 8×8 and 5×5 supercells of graphene to simulate different concentrations of pesticides and water molecules interacting with it, and include a vacuum up to 22 Å (minimum thickness of vacuum was 12.8 Å) in the direction perpendicular to the graphene plane to keep interactions between periodic images of molecules minimal. Integrations over the Brillouin zone (for these periodic supercells) were sampled with $3 \times 3 \times 1$ and $1 \times 1 \times 1$ uniform meshes of k-points, ensuring convergence with respect to k-points while using occupation numbers smeared with Fermi–Dirac scheme with a broadening of 0.003 Ry. We considered many structural configurations for each pesticide (β -ES, CP, and ML) obtained with different orientations and positions of the pesticides and water molecules relative to graphene, and relaxed the structure to minimize the energy until Hellman Feynman forces on atoms were less than 0.001 Ry/bohr in magnitude.

Supporting Information

Supporting Information is available from the Wiley Online Library or from the author

Acknowledgements

Authors thank the Nano Mission of the Department of Science and Technology (DST), Government of India for supporting our research program. Authors thank EWRE Division, Department of Civil Engineering, IIT Madras for providing some analytical facilities. UVW acknowledges funding from AOARD grants FA2386-10-1-4062 and FA2386-10-1-4150.

- [1] Y. Matsui, D. R. U. Knappe, K. Iwaki, H. Ohira, *Environ. Sci. Technol.* **2002**, *36*, 3432.
- [2] T. Pradeep, Anshup, *Thin Solid Films* **2009**, *517*, 6441.
- [3] A. K. Leight, R. F. Van Dolah, *Environ. Toxicol. Chem.* **1999**, *18*, 958.
- [4] S. L. Simonich, R. A. Hites, *Science* **1995**, *269*, 1851.
- [5] A. S. Nair, T. Pradeep, *Curr. Sci.* **2003**, *84*, 1560.
- [6] W. Chen, L. Duan, D. Zhu, *Environ. Sci. Technol.* **2007**, *41*, 8295.
- [7] D. Lin, B. Xing, *Environ. Sci. Technol.* **2008**, *42*, 7254.
- [8] G.-C. Chen, X.-Q. Shan, Z.-G. Pei, H. Wang, L.-R. Zheng, J. Zhang, Y.-N. Xie, *J. Hazard. Mater.* **2011**, *188*, 156.
- [9] M. L. Schipper, N. Nakayama-Ratchford, C. R. Davis, N. W. S. Kam, P. Chu, Z. Liu, X. Sun, H. Dai, S. S. Gambhir, *Nat. Nanotechnol.* **2008**, *3*, 216.
- [10] A. Magrez, S. Kasas, V. Salicio, N. Pasquier, J. W. Seo, M. Celio, S. Catsicas, B. Schwaller, L. Forró, *Nano Lett.* **2006**, *6*, 1121.
- [11] K. S. Novoselov, A. K. Geim, S. V. Morozov, D. Jiang, Y. Zhang, S. V. Dubonos, I. V. Grigorieva, A. A. Firsov, *Science* **2004**, *306*, 666.
- [12] N. Kurra, A. A. Sagade, G. U. Kulkarni, *Adv. Funct. Mater.* **2011**, *21*, 3836.
- [13] S. Stankovich, D. A. Dikin, G. H. B. Dommett, K. M. Kohlhaas, E. J. Zimney, E. A. Stach, R. D. Piner, S. T. Nguyen, R. S. Ruoff, *Nature* **2006**, *442*, 282.
- [14] A. K. Geim, *Science* **2009**, *324*, 1530.
- [15] Z. Liu, J. T. Robinson, X. Sun, H. Dai, *J. Am. Chem. Soc.* **2008**, *130*, 10876.
- [16] F. Schedin, A. K. Geim, S. V. Morozov, E. W. Hill, P. Blake, M. I. Katsnelson, K. S. Novoselov, *Nat. Mater.* **2007**, *6*, 652.
- [17] R. S. Sundaram, C. Gómez-Navarro, K. Balasubramanian, M. Burghard, K. Kern, *Adv. Mater.* **2008**, *20*, 3050.
- [18] L. Tang, Y. Wang, Y. Li, H. Feng, J. Lu, J. Li, *Adv. Funct. Mater.* **2009**, *19*, 2782.
- [19] N. Jung, A. C. Crowther, N. Kim, P. Kim, L. Brus, *ACS Nano* **2010**, *4*, 7005.
- [20] C. N. R. Rao, A. K. Sood, K. S. Subrahmanyam, A. Govindaraj, *Angew. Chem., Int. Ed.* **2009**, *48*, 7752.
- [21] G. K. Dimitrakakis, E. Tylianakis, G. E. Froudakis, *Nano Lett.* **2008**, *8*, 3166.
- [22] C. Liu, F. Li, L.-P. Ma, H.-M. Cheng, *Adv. Mater.* **2010**, *22*, E28.
- [23] D. R. Dreyer, H.-P. Jia, C. W. Bielawski, *Angew. Chem., Int. Ed.* **2010**, *49*, 6813.
- [24] Y. Zhu, S. Murali, W. Cai, X. Li, J. W. Suk, J. R. Potts, R. S. Ruoff, *Adv. Mater.* **2010**, *22*, 3906.
- [25] W. Hu, C. Peng, W. Luo, M. Lv, X. Li, D. Li, Q. Huang, C. Fan, *ACS Nano* **2010**, *4*, 4317.
- [26] J. Chen, J. Zou, J. Zeng, X. Song, J. Ji, Y. Wang, J. Ha, X. Chen, *Anal. Chim. Acta* **2010**, *678*, 44.
- [27] T. S. Sreeprasad, S. M. Maliyekkal, K. Deepti, K. Chaudhari, P. L. Xavier, T. Pradeep, *ACS Appl. Mater. Interfaces* **2011**, *3*, 2643.
- [28] V. Chandra, J. Park, Y. Chun, J. W. Lee, I.-C. Hwang, K. S. Kim, *ACS Nano* **2010**, *4*, 3979.
- [29] T. S. Sreeprasad, S. M. Maliyekkal, K. P. Lisha, T. Pradeep, *J. Hazard. Mater.* **2011**, *186*, 921.
- [30] W. Gao, M. Majumder, L. B. Alemany, T. N. Narayanan, M. A. Ibarra, B. K. Pradhan, P. M. Ajayan, *ACS Appl. Mater. Interfaces* **2011**, *3*, 1821.
- [31] G. Zhao, L. Jiang, Y. He, J. Li, H. Dong, X. Wang, W. Hu, *Adv. Mater.* **2011**, *23*, 3959.
- [32] a) J. Weber, C. J. Halsall, D. Muir, C. Teixeira, J. Small, K. Solomon, M. Hermanson, H. Hung, T. Bidleman, *Sci. Total Environ.* **2010**, *408*, 2966; b) X. Zhao, H.-M. Hwang, *Arch. Environ. Con. Tox.* **2009**, *56*, 646; c) H. Sujatha, S. M. Nair, J. Chacko, *Water Res.* **1999**, *33*, 109; d) M. Kumar, L. Philip, *Chemosphere* **2006**, *62*, 1064; e) B. K. Singh, A. Walker, J. A. W. Morgan, D. J. Wright, *Appl. Environ. Microb.* **2004**, *70*, 4855.
- [33] a) S. Memon, N. Memon, S. Memon, Y. Latif, *J. Hazard. Mater.* **2011**, *186*, 1696; b) T. Siddique, B. C. Okeke, M. Arshad, W. T. Frankenberger, *J. Agric Food Chem.* **2003**, *51*, 8015.
- [34] a) A. K. Leight, R. F. V. Dolah, *Environ. Toxicol. Chem.* **1999**, *18*, 958; b) T. Holland, G. Windham, P. Kolachana, F. Reinisch, S. Parvatham, A. M. Osorio, M. T. Smith, *Mutat. Res.-Gen. Tox. En.* **1997**, *388*, 85; c) H. Wu, R. Zhang, J. Liu, Y. Guo, E. Ma, *Chemosphere* **2011**, *83*, 599.
- [35] W. Chen, L. Yan, P. R. Bangal, *J. Phys. Chem. C* **2010**, *114*, 19885.
- [36] T. S. Sreeprasad, A. K. Samal, T. Pradeep, *J. Phys. Chem. C* **2009**, *113*, 1727.
- [37] A. J. Gil, S. Adhikari, F. Scarpa, J. Bonet, *J. Phys.: Condens. Matter.* **2010**, *22*, 145302.
- [38] P. C. Mishra, R. K. Patel, *J. Hazard. Mater.* **2008**, *152*, 730.
- [39] A. H. Yonli, I. Batonneau-Gener, J. Koulidiati, *J. Hazard. Mater.* **2012**, *203–204*, 357.
- [40] S. Kushwaha, G. Sreelatha, P. Padmaja, *J. Chem. Eng. Data* **2011**, *56*, 2407.
- [41] J. Carriger, G. Rand, *Ecotoxicology* **2008**, *17*, 660.
- [42] H. Goebel, S. Gorbach, W. Knauf, R. H. Rimpau, H. Huttenbach, *Residue Rev.* **1982**, *83*, 1.

- [43] M. Manes, in *Encyclopedia of Environmental Analysis and Remediation*, (Ed: R. A. Mayer), Wiley, New York **1998**, 26–68.
- [44] Y. Yang, Y. Chun, G. Sheng, M. Huang, *Langmuir* **2004**, *20*, 6736.
- [45] G. Lagaly, *Appl. Clay Sci.* **2001**, *18*, 205.
- [46] F. Tuinstra, *J. Chem. Phys.* **1970**, *53*, 1126.
- [47] R. G. Baughman, S. K. Jorgensen, R. A. Jacobson, *J. Agric. Food Chem.* **1978**, *26*, 576.
- [48] G. Smith, C. Kennard, K. Shields, *Aust. J. Chem.* **1977**, *30*, 911.
- [49] N. I. Kovtyukhova, P. J. Ollivier, B. R. Martin, T. E. Mallouk, S. A. Chizhik, E. V. Buzaneva, A. D. Gorchinskiy, *Chem. Mater.* **1999**, *11*, 771.
- [50] D. Li, M. B. Muller, S. Gilje, R. B. Kaner, G. G. Wallace, *Nat. Nanotechnol.* **2008**, *3*, 101.
- [51] Y. Zhou, Q. Bao, L. A. L. Tang, Y. Zhong, K. P. Loh, *Chem. Mater.* **2009**, *21*, 2950.
- [52] S. Baroni, S. de Gironcoli, A. Dal Corso, P. Giannozzi, *Rev. Mod. Phys.* **2001**, *73*, 515.
- [53] D. Vanderbilt, *Phys. Rev. B* **1990**, *41*, 7892.
- [54] J. P. Perdew, K. Burke, M. Ernzerhof, *Phys. Rev. Lett.* **1996**, *77*, 3865.

Received: May 23, 2012
Revised: August 6, 2012
Published online: September 24, 2012